typeset using JPSJ.sty <ver.1.0b>

Magnetism of Geometrically Frustrated Metallic Compounds

Masayuki Shiga and Hiroyuki Nakamura

Department of Materials Science and Engineering, Kyoto University, Kyoto 606-8501

(Received December 15, 2000)

Frustration of magnetic interactions gives rise to various anomalies in the magnetic structure and the critical behavior at the transition temperature. Experimental studies on frustration have been focussed on ionic crystals so far. We present some experimental investigations of geometrically frustrated metallic compounds and show that the frustration plays an important role even in the itinerant electron systems. As examples, spin liquid characters of Y(Sc)Mn_2, a spin-liquid–spin-glass transition in the Y(Sc)$(Mn_{1-x}Al_x)_2$ system and a possible orbital-ordered spin-singlet state in triangular-lattice vanadium sulphide $BaVS_3$ are discussed.

KEYWORDS: frustration, spin fluctuations, spin liquid, itinerant electron, YMn_2, $BaVS_3$

§1. Introduction

Frustration of magnetic interactions gives rise to various exotic phenomena in the ground-state properties and at the magnetic critical point.[1)] Among them, the ground state of the fully frustrated (FFR) systems, which is characterized by the existence of macroscopic number of degenerate spin configurations, are attracting much attention as a candidate of novel quantum states such as a spin liquid state. FFR systems are realized in antiferromagnetically interacting spins placed on a special geometry like two-dimensional (2D) and three-dimensional (3D) triangular-based lattices as shown in Fig. 1.

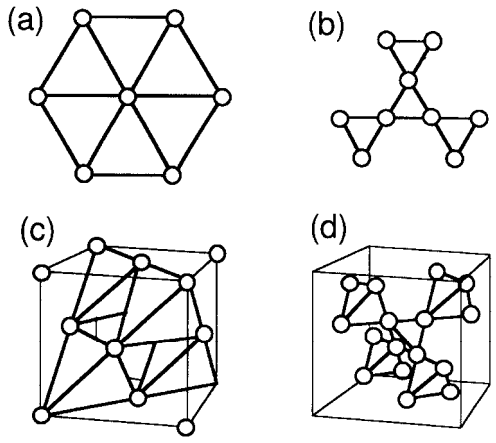

Fig. 1. Geometrically frustrated lattices; (a) edge-sharing triangular lattice, (b) corner-sharing triangular (Kagomé) lattice, (c) edge-sharing tetrahedral (FCC) lattice and (d) corner-sharing tetrahedral lattice.

The most important subject in this field is certainly to find out the quantum spin liquid (QSL) state, which is characterized by strong spin fluctuations with antiferromagnetic correlation. Theoretically, the concept of the resonating valence bond (RVB) state,[2)] which may be regarded as a QSL state, was proposed as the singlet ground state of 2D triangular lattice of antiferromagnetic Ising spins. So far, studies on FFR systems have been most extensively carried out for ionic crystals, for instance, $CsCoCl_3$ type compounds as the candidate for 2D triangular lattice (Fig. 1 (a)), $SrCr_{9p}Ga_{12-9p}O_{19}$ with 2D Kagomé lattice (corner-sharing triangular lattice, Fig. 1 (b)) and pyrochlore compounds composed of corner-sharing tetrahedrons (Fig. 1 (d)) as a typical candidate for 3D frustrated system. However, in most cases, a magnetically ordered phase is formed at low temperatures. On the other hand, metallic magnetic systems have not been intensively studied from the view point of frustration. In fact, it is difficult to suppose the spin frustration in itinerant electron systems, at least, in the Hartree-Fock limit. On the basis of the spin fluctuation (SF) theory,[3)] however, there is no reason why the frustration does not play an important role in the strongly correlated itinerant electron systems.

Figure 2 schematically illustrates magnetic phases and the magnitude of local magnetic moment, or in other word, the amplitude of local spin fluctuations, as a function of t/U, where U is the intra-atomic correlation energy and t the transfer integral. (We use t/U as the horizontal axis in the figure to avoid divergence of U/t in the local moment limit but discuss U/t in the text to refer the strength of the correlation effect.) Before the concept of SF has been introduced, itinerant-electron and local-moment systems are clearly separated from each other as shown in Fig. 2 (a). In the itinerant-electron side, a magnetically ordered state appears if the Stoner (or Lidiard) condition is fulfilled ($U/t > 1$), and T_C (or T_N) and the spontaneous (sublattice) moment increases with increasing U/t. For $U/t < 1$, the ground state is a merely (exchange enhanced) Pauli paramagnet.

It is difficult to take into consideration the role of frustration in this picture. The SF theory has greatly modified this scheme as shown in Fig. 2 (b). The critical value of U/t and the critical temperature (T_C or T_N) are suppressed from the Stoner criterion. For a system with-

out frustration, the paramagnetic phase near the phase boundary is characterized by the existence of long wave length SF, even at 0 K as zero-point SF. With increasing U/t, the amplitude of SF increases and the spatial distribution becomes local moment-like. Thus, the gap between itinerant-electron and local-moment systems disappears.

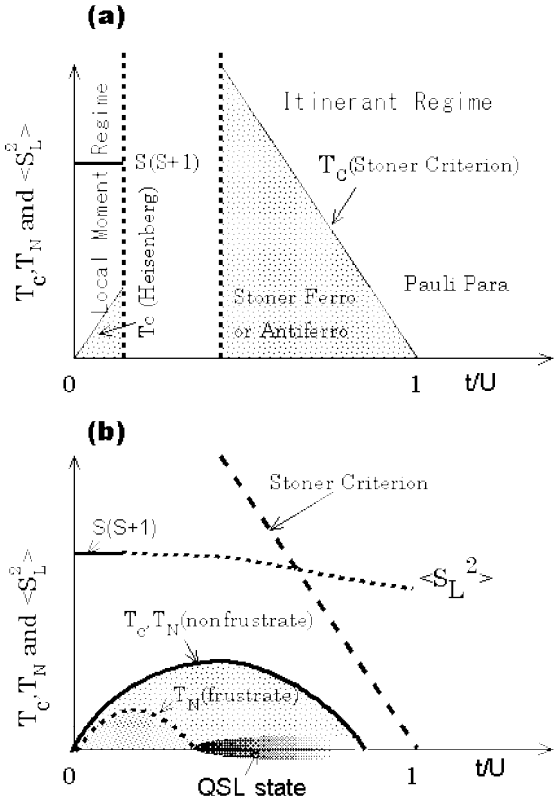

Fig. 2. Schematic diagram of magnetic phases and the magnitude of local moment $\langle S_L^2 \rangle$ as functions of the inverse relative correlation energy to the transfer integral t/U. (a) Classical model: The Heisenberg model for a localized moment system. (t corresponds to the inter-atomic exchange integral and $\langle S_L^2 \rangle$ to the Hund rule value $S(S+1)$); the Stoner (Lidiard) model for an itinerant system. The phase boundary is determined by the Stoner criterion. (b) Unified model: The ordered phase is considerably reduced from the Stoner criterion by taking account of SF. For an ideal fully frustrated system, no ordered state appears and the ground state is QSL. The frustration in the real system remarkably reduces the ordered region. The ground state of non-magnetic region, near the boundary at least, can be regarded as also QSL state. $\langle S_L^2 \rangle_{\text{total}}$ would continuous to $S(S+1)$ value of the local moment limit.

In this picture, RVB or QSL state is also expected in itinerant systems with geometrical frustration, at least in a large U/t region. Starting from a weak correlation limit, frustration suppresses the formation of a magnetically ordered state and so the critical t/U for an ordered state shifts far left as shown in Fig. 2 (b). Then, we can expect giant and spatially localized zero point SF for the paramagnetic ground state near the phase boundary, which can be regarded as QSL state. We should say that the transfer integral t would help the formation of QSL state so that the non-magnetic ground state of frustrated itinerant systems should have more or less spin liquid characters. Furthermore, recent developments of the research on transition metal oxides including superconducting cuprates, which are typical highly correlated electron systems, have revealed a wide spectrum of exotic phenomena, including superconductivity, field-induced metal-insulator transition, etc. These materials should locate just near the boundary between local moment and itinerant electron regimes. It is plausible that the geometrical spin frustration plays an important role in giving rise to exotic ground states and remarkable phase transitions.

Here, we will review two examples of our resent investigations on the geometrically frustrated strongly correlated electron systems. One is YMn_2 based compounds, in which Mn atoms compose corner-shearing tetrahedrons. The other is $BaVS_3$, which has the $CsCoCl_3$-type structure at room temperature and so V atoms form the triangular lattice in the c plane.

§2. YMn_2 system

2.1 Spin-liquid properties of $Y(Sc)Mn_2$ and $Y(Lu)Mn_2$

2.1.1 Macroscopic properties

YMn_2 has the C15 Laves phase structure, where Mn atoms form a network of corner-sharing tetrahedrons. Mn-Mn interaction is antiferromagnetic and, therefore, it can be regarded as a typical FFR system. At ambient pressure, it becomes antiferromagnetic below 100 K accompanied with a huge volume expansion and a tetragonal distortion. The spin structure is not a simple collinear one but helically modulated with an extremely long period of 400 Å.[4] The origin of this super-long period helical modulation itself is an interesting problem and probably relates to frustration, which was discussed elsewhere.[5]

The antiferromagnetic state is unstable and highly sensitive to pressure or to impurity. By substituting 3% Sc for Y, which reduces its lattice constant a little, the paramagnetic state is stabilized down to the lowest temperature.[6] The paramagnetic state is not a simple Pauli paramagnet but exhibits several anomalies such as an extraordinary large low-temperature specific heat of $\gamma = 150$ mJ/K^{2}mol, being comparable to a heavy fermion system.[7] The antiferromagnetic state also disappears by applying a rather small pressure, say only 2 kbar.[8] Again, the γ value is strongly enhanced by more than 10 times compared with that of antiferromagnetic state. The γ value decreases with increasing pressure. The temperature dependence of the electrical resistivity is concave upward. The coefficient of the T^2 term, A, is also extremely large in accordance with the enhancement of the γ value.[9]

It is interesting to compare the magnetic specific heat and the entropy of antiferromagnetic YMn_2 and paramagnetic $Y(Sc)Mn_2$. Figure 3 shows the result of specific heat measurements up to 300 K for both the compounds.[10] By subtracting the phonon and ordinary electronic contributions to the specific heat, we have esti-

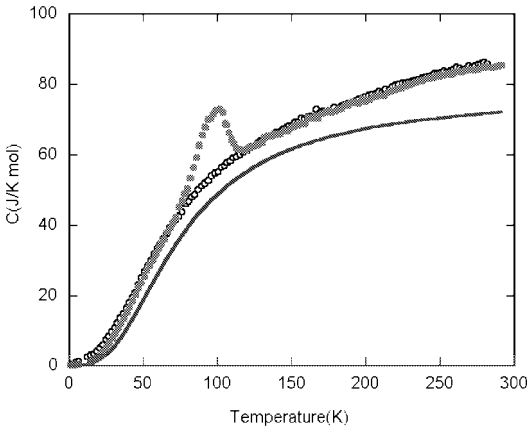

Fig. 3. Specific heat of $Y_{1-x}Sc_xMn_2$, $x = 0$ (•), $x = 0.03$ (○). The solid curve is the non-magnetic specific heat for $Y_{1-x}Sc_xMn_2$ estimated by using the Debye function with $\Theta_D = 304$ K

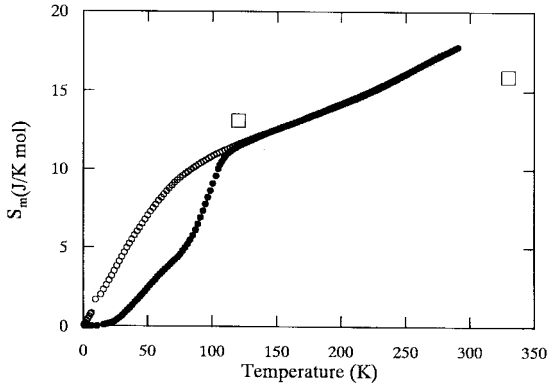

.

Fig. 4. The temperature dependence of the magnetic entropy for $Y_{1-x}Sc_xMn_2$, $x = 0$ (•), $x = 0.03$ (○). Open squares are estimated from neutron scattering data for $Y_{1-x}Sc_xMn_2$ at 120 and 330 K

mated the magnetic entropy, S_m, for both compounds. The results are shown in Fig. 4. The magnetic entropy of YMn_2 gradually increases, followed by an abrupt rise in the temperature range of 80–120 K, which is due to the magnetic transition. Above T_N, S_m increases with increasing temperature. This is reasonably ascribed to the thermal excitations of SF. On the other hand, $Y_{0.97}Sc_{0.03}Mn_2$ shows a rapid increase in S_m below 100 K. Above, 120 K, S_m of both the compounds coincides each other. These results indicate that the paramagnetic state of the two compounds is equivalent from the thermodynamical point of view, which means the same amplitude of SF for both the compounds at high temperatures. Therefore, the entropy change due to antiferromagnetic transition, which was observed in YMn_2, has to be released at low temperatures below 100 K in $Y_{0.97}Sc_{0.03}Mn_2$, as the increase of entropy due to thermal excitations of SF, resulting in the enhancement of the γ value. It is interesting to note that the absolute value of S_m at 300 K approximately corresponds to $S = 1$ spin entropy. Thus, the enhancement of γ and A values implies the existence of large amplitude of SF even at low temperatures.

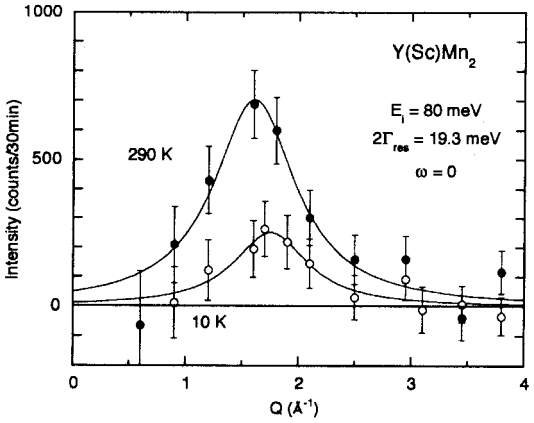

Fig. 5. Magnetic neutron scattering rate of $Y(Sc)Mn_2$ as a function of wave vector Q at zero energy transfer with an energy resolution of $2\Gamma_{res} = 19.3$ meV at 10 K (○) and 290 K (•).

2.1.2 Neutron scattering of $Y(Sc)Mn_2$

In order to detect SF, we have performed paramagnetic neutron scattering experiments using polarized neutron beam.[12] Figure 5 shows the quasi-elastic Q-scan spectra with an energy window of $2\Gamma_{res} = 20$ meV for $Y_{0.97}Sc_{0.03}Mn_2$ at 10 and 290 K. A large scattering was observed centered around $Q = 1.6$ Å^{-1}. The corresponding wave length is approximately twice of the Mn inter-atomic distance, indicating antiferromagnetic correlation of SF. It should be noted that large scattering is observed even at 10 K, suggesting the existence of strong zero-point SF with antiferromagnetic correlation. This interpretation is confirmed by the energy spectrum, which is shown in Fig. 6. At 10 K, scattering was observed only on the neutron energy-loss side ($\omega > 0$), implying the absence of thermally excited SF. The width of the spectra is approximately 20 meV (200 K), indicating the characteristic frequency of zero-point SF of 5×10^{12} Hz. At high temperatures, the scattering amplitude increases on both side, indicating an increase of thermally excited SF. From the integrated intensity of scattering, we have roughly estimated the local amplitude of SF as 1.2 μ_B at 10 K and 1.5 μ_B at 290 K. This value approximately agrees with that estimated from the magnetic entropy as seen in Fig. 4. We believe that these observations indicate a spin-liquid character of paramagnetic YMn_2. At 0 K, SF are purely quantum ones and in this sense, we may regard the ground state being in QSL state.

Recently, Ballou et al.[13] have carried out neutron scattering experiments using a single crystal of $Y(Sc)Mn_2$ and revealed that SF exhibit anisotropic distribution in the reciprocal space. Lacroix et al.[14] have shown that these anisotropic SF are characteristic of the pyrochlore structure and can be ascribed to the 4-sites spin singlet state formed within a tetrahedron.

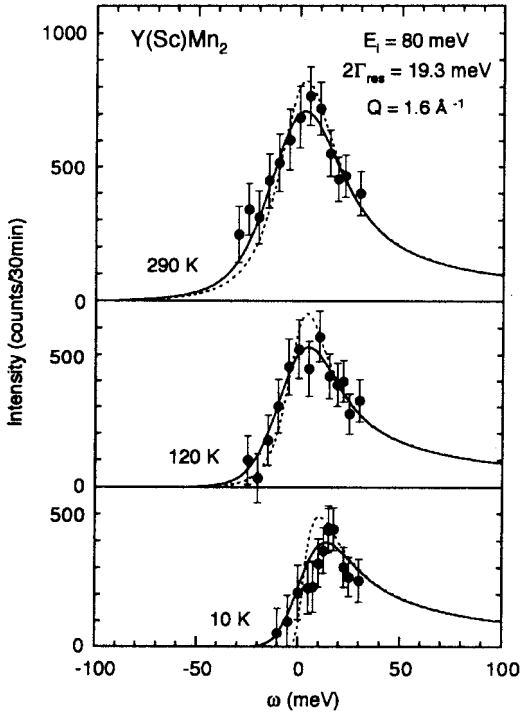

Fig. 6. Magnetic neutron scattering rate of Y(Sc)Mn2 as a function of energy transfer measured for a momentum transfer of $Q = 1.6$ Å. Dashed curves indicate deconvoluted values.

2.1.3 Nuclear spin relaxation in Y(Lu)Mn_2

Canals and Lacroix[14] have shown that these anisotropic SF can be expressed by the generalized susceptibility as

$$\chi^{-1}(Q+q,\omega) = \chi_{\mathrm{Q}}^{-1} + a_1(q_{\mathrm{x}}^2 + q_{\mathrm{y}}^2) + a_2 q_{\mathrm{z}}^4 - i\omega/\Gamma. \quad (2.1)$$

For these anisotropic SF, Lacroix et al.[15] calculated the temperature dependence of the nuclear spin-lattice relaxation time T_1 and obtained an expression as

$$1/T_1 \propto T\chi(Q)^{3/4}. \quad (2.2)$$

Using the Curie-Weiss relation for the staggered susceptibility, we have

$$1/T_1 \propto T/(T+\Theta)^{3/4}. \quad (2.3)$$

Except at very low temperatures, the spin-spin relaxation time, T_2, is also mediated by SF, then it is plausible that T_2 is proportional to T_1. In order to confirm this prediction, we have carefully measured the temperature dependence of T_2 of $Y_{0.96}Lu_{0.04}Mn_2$ (We doped Lu instead of Sc to stabilize the paramagnetic state since we can avoid the overlap of Sc and Mn NMR signals). The result is shown in Fig. 7.

As seen in the figure, we have fairly good fitting by eq. (2.3), supporting the spin-liquid character of SF in this system.

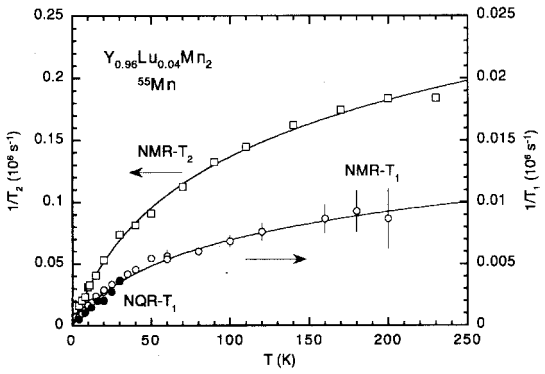

Fig. 7. Temperature dependence of the nuclear spin-spin relaxation rate $1/T_2$ (squares), spin-lattice relaxation rate $1/T_1$ measured by ^{55}Mn NMR (○) and by ^{55}Mn NQR (●) of Y(Lu)Mn_2. The solid curve indicates fitting by eq. (2.3).

2.2 Spin-liquid–spin-glass transition in Y(Sc)($Mn_{1-x}Al_x$)$_2$

The frustrated system is highly sensitive to impurity because the ground state degeneracy can be removed by introducing nonmagnetic sites, giving rise to a spin-glass state. We have prepared $Y_{0.97}Sc_{0.03}(Mn_{1-x}Al_x)_2$ pseudo-binary compounds and studied their magnetic properties. Figure 8 shows the temperature dependence of susceptibility. The susceptibility increases with increasing x and approaches a Curie-Weiss type at high temperatures. For $x > 0.05$, a maximum is observed in $\chi - T$ curves at low temperatures for zero-field-cooled samples but not for field-cooled samples, suggesting spin-glass freezing. These results confirm the frustrated nature of the present system and indicate the spin-liquid–spin-glass transition by introducing impurity.

Figure 9 depicts the concentration dependence of the electronic specific heat coefficient, γ, of Y(Sc)($Mn_{1-x}Al_x$)$_2$. The γ value decreases rapidly with increasing x and approaches a normal value in the spin-glass region, $x > 0.05$. This behavior will be discussed in the next subsection in terms of SF.

The direct evidence for the spin-liquid–spin-glass transition is obtained by performing paramagnetic neutron scattering experiments to observe SF.[12] Figure 10 shows the result of the Q-scan for Y(Sc)($Mn_{0.9}Al_{0.1}$)$_2$ with an energy window of 5.8 meV obtained at 10, 120 and 290 K. The spectrum at 290 K is similar to that for Y(Sc)Mn_2 with a broad peak at around $Q = 1.6$ Å^{-1}, although the intensity is much smaller due to the narrower energy window. In contrast to the result for Y(Sc)Mn_2, the scattering amplitude increases with decreasing temperature. At 10 K, a double peak structure similar to that of the elastic neutron diffraction pattern was observed.

Figure 11 shows energy spectra of Y(Sc)($Mn_{0.9}Al_{0.1}$)$_2$ measured at $Q = 1.6$ Å^{-1}. The profile of the spectrum at 290 K is again similar to that for Y(Sc)Mn_2 with nearly the same line width. With decreasing temperature, however, the line width decreases rapidly and approaches the energy resolution limit of the spectrometer at 10 K. This

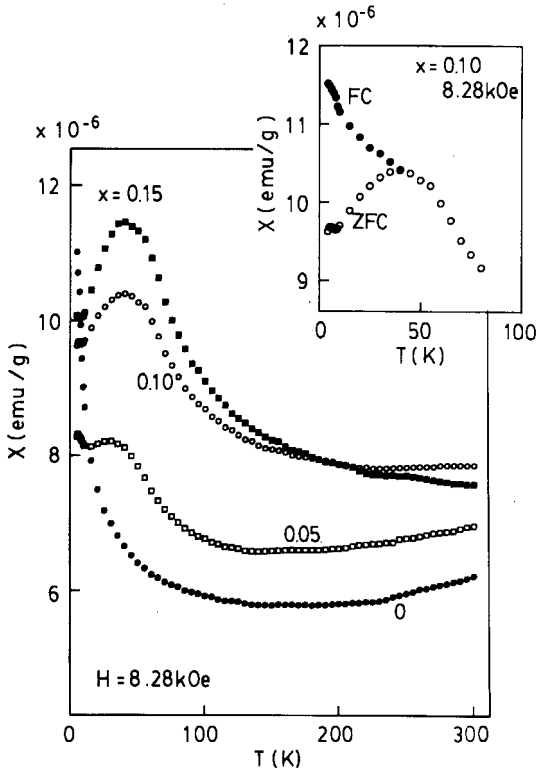

Fig. 8. Temperature dependence of susceptibility of $Y_{0.97}Sc_{0.03}(Mn_{1-x}Al_x)_2$. The inset shows field cooled and zero-field cooled curves for $x = 0.1$.

result shows that SF in the Al-substituted compound are strongly suppressed at low temperatures, as expected for the spin-glass freezing at low temperatures. The increase of scattering amplitude with decreasing temperature in the quasi-elastic Q-scan measurements can be simply explained in terms of narrowing of the energy spectra.

The spin-glass transition of $Y(Sc)(Mn_{0.9}Al_{0.1})_2$ was also detected by muon spin relaxation.[16] Figure 12 shows the temperature dependence of muon spin relaxation rate in $Y_{0.97}Sc_{0.03}Mn_2$ and $Y_{0.97}Sc_{0.03}(Mn_{0.9}Al_{0.1})_2$ measured in a small longitudinal magnetic field of 10 mT applied to surpress the nuclear moment fluctuations. The relaxation rate of $Y_{0.97}Sc_{0.03}(Mn_{0.9}Al_{0.1})_2$ exhibits a sharp peak at around 45 K, which corresponds to the susceptibility maximum, indicating a fairly sharp spin-glass transition in this sample. It should be noted, however, the relaxation rate of $Y_{0.97}Sc_{0.03}Mn_2$ also show a broad maximum at around 2.5 K, where no anomaly is observed in susceptibility measurement. Noting the magnitude of peak height and performing other quantitative analyses, we have concluded that majority of Mn tetrahedrons are singlets in the ground state whereas the remaining paramagnetic tetrahedrons are frozen randomly at 2.5 K, producing the internal field at the stopped μ^+ site at low temperatures. The paramagnetic tetrahedrons are probably associated with some imperfections of the lattice such as Sc atoms at Y sites. If this is the case, the ideal corner-sharing tetrahedral lattice without imperfection would be in an entirely singlet ground state and in QSL state.

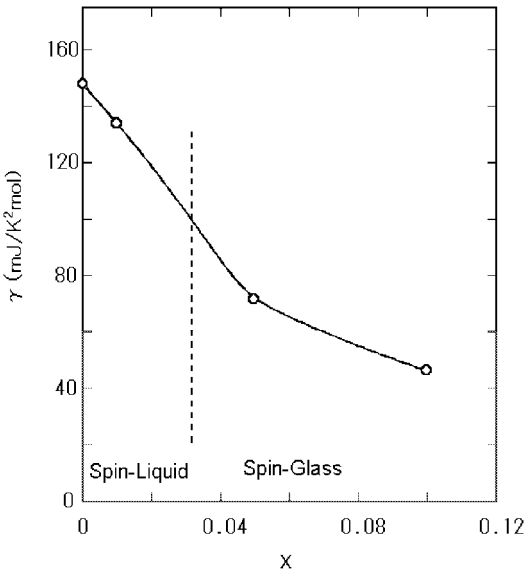

Fig. 9. Concentration dependence of the electronic specific heat coefficient, γ of $Y(Sc)(Mn_{1-x}Al_x)_2$.

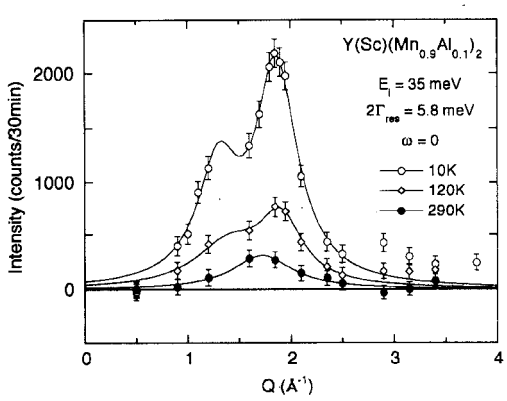

Fig. 10. Magnetic neutron scattering rate of $Y(Sc)(Mn_{0.9}Al_{0.1})_2$ as a function of wave vector Q at zero energy transfer with energy resolution of $2\Gamma_{res} = 19.3$ meV at 290 K (•), 120 K (◇) and 10 K (○). Solid curves are guide for eyes.

2.3 Spin fluctuations in $Y_{0.97}Sc_{0.03}(Mn_{1-x}Al_x)_2$

The spin-liquid–spin-glass transition may be interpreted in terms of SF theory as follow: From neutron scattering spectra, we can draw the characteristic feature of SF spectra for $Y(Sc)Mn_2$ and $Y(Sc)(Mn_{0.9}Al_{0.1})_2$ as shown in Fig. 13. For $Y(Sc)Mn_2$, there is no static SF and the spectrum distributes most densely in the rather low energy range compared with the band width, W, at around thermal energy of room temperature. Therefore, SF at 0 K are totally of quantum ones, implying the quantum spin-liquid nature of the ground state.

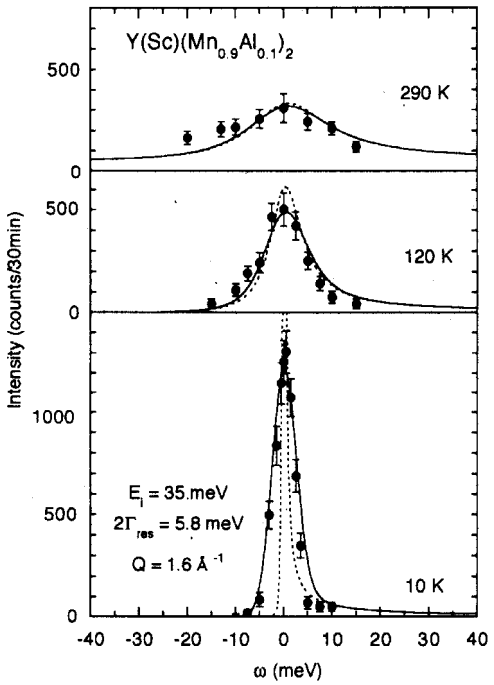

Fig. 11. Magnetic neutron scattering rate of $Y(Sc)(Mn_{0.9}Al_{0.1})_2$ as a function of energy transfer measured for a momentum transfer of $Q = 1.6$ Å^{-1}.

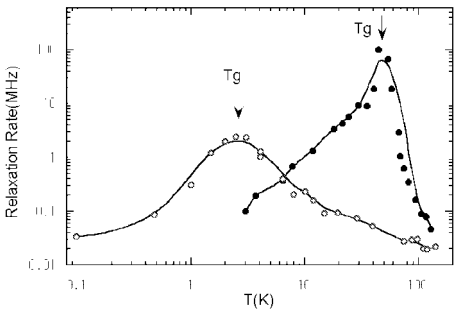

Fig. 12. The temperature dependence of muon spin relaxation rate in $Y_{0.97}Sc_{0.03}Mn_2$ (○) and $Y_{0.97}Sc_{0.03}(Mn_{0.9}Al_{0.1})_2$ (●) measured in the longitudinal magnetic field of 10 mT.

With increasing temperature, low lying components of SF are easily excited by thermal energy, giving rise to rapid growth of thermal SF, which accompany the increase of magnetic entropy, resulting in the enhancement of low temperature specific heat as schematically shown in Fig. 14. Here, we put $\langle S_L^2 \rangle_{tot}$ being constant according to Takahashi's assumption.[17] On the other hand, for $Y(Sc)(Mn_{0.9}Al_{0.1})_2$, SF spectrum has the static component, giving rise to the spin-glass ground state. Therefore, the contribution of thermal SF is far smaller than those for $Y(Sc)Mn_2$ as seen in Fig. 14. As a result, the low temperature specific heat becomes normal.

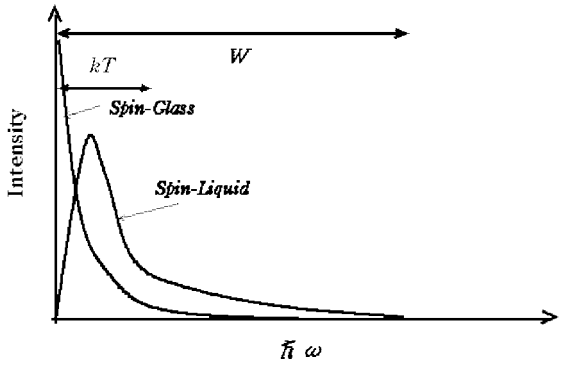

Fig. 13. Schematic diagram of energy spectra of spin fluctuations for spin liquid and spin glass systems. W represents the band width.

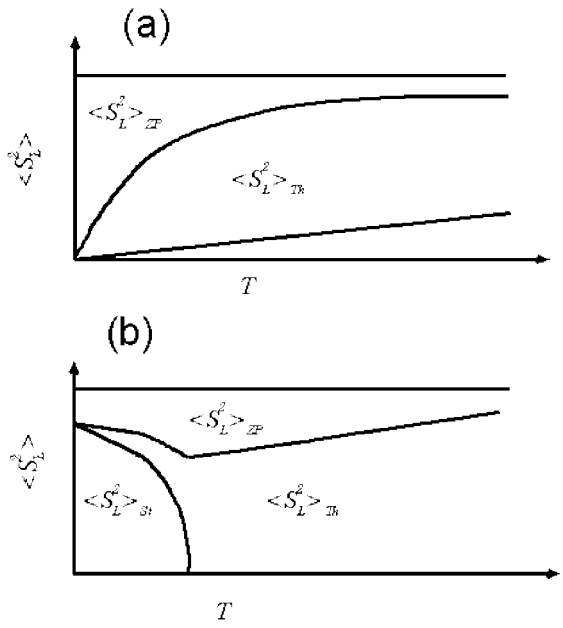

Fig. 14. Schematic diagram of the temperature dependence of local amplitude of spin fluctuations for (a) spin-liquid and (b) spin-glass systems.

Finally, we would like to add a comment that macroscopic and microscopic behaviors of β-$Mn_{1-x}Al_x$ alloys are almost same as those of in $Y_{0.97}Sc_{0.03}(Mn_{1-x}Al_x)_2$. We have discussed that the Mn II site of β-Mn consists of corner sharing triangles and so that these behaviors are well understood in the same context.[18]

§3. $BaVS_3$: orbital-ordered spin-singlet state

Recently, variety of exotic phenomena such as High-T_c, Metal-Insulator transition and CMR have been found in transition metal oxides and calcogenides, which are typical strongly correlated electron systems and locate at around the boundary between local moment and itinerant electron regimes. Spin frustration may play an important role in manifesting new phenomena along with orbital degeneracies.

Pen et al.[19] theoretically treated the orbital degree of

freedom in 2D triangular lattice and discussed the possibility of a spin-singlet formation accompanied by orbital ordering in d^1 ($S = \frac{1}{2}$) and d^2 ($S = 1$) system with orbital degeneracy. In this model, the frustration of the spin component is essential. It is interpreted that the orbital-ordered spin-singlet state may be realized when the potential energy gain by the quenching of the frustrated spins overcomes the energy loss due to the local lattice distortion associated with the orbital ordering. Substantial d electron transfer (inter-site hybridization), i.e., a certain extent of metallic nature, is necessary to realize the state. The dimer and trimer formation are expected for the $S = \frac{1}{2}$ and $S = 1$ cases, respectively. This fascinating scenario adds a new physical mechanism in the spin-singlet formation. Therefore, it is of interest to search actual prototypes; Pen et al.[19] developed this model to explain the trimer formation in a triangular lattice $LiVO_2$.

We apply this model to some vanadium sulphides. Generally, since sulphur has strong covalency with transition metal elements, sulphides may be more hopeful candidates than oxides. We present here $BaVS_3$ as an example of the $S = \frac{1}{2}$ system.[20]

$BaVS_3$ is known to exhibit a metal-insulator transition at $T_{MI} \simeq 70$ K (metallic above T_{MI} and insulating below T_{MI}). The crystal structure at high temperatures, shown in Fig. 15, is the hexagonal perovskite $CsCoCl_3$-type with space group $P6_3/mmc$, in which V atoms ($2a$ site) form 1D chains along the c direction and a triangular lattice in the c plane.

Since the intra-chain V-V distance ($\simeq 2.8$ Å) is much smaller than the intra-chain separation ($\simeq 6.7$ Å) and nearly equal to the V metallic distance, $BaVS_3$ has been considered as a prototype for the 1D system. However, conductivity measurements using a single crystal has revealed that the conductivity in the c plane is considerable, implying inter-chain electron hopping.[21] Moreover, recent neutron scattering experiments showed that the inter-chain antiferromagnetic coupling is rather dominant, suggesting that the spin frustration on the c-plane triangular lattice is crucial.[22]

The V atom is surrounded by a nearly regular octahedron formed by S atoms, resulting in triply degenerate t_{2g} states as the crystal field ground state. Below $T_S \simeq 240$ K, it shows a small orthorhombic structural deformation, resulting in a slightly zigzag configuration of the V chains.[23] The magnetic susceptibility, presented in Fig. 16, shows a sharp peak at T_{MI} and drops rapidly in the insulating state below T_{MI}. A considerable upturn at low temperatures was reported for all previous measurements, but not in ours. In $BaVS_3$, S deficiency results in an appearance of ferromagnetic-like components, then the controlling of the stoichiometry seems to be very important to extract the real ground state.

Although the temperature dependence of susceptibility looks like that of an antiferromagnet, a precise neutron diffraction experiment failed to detect long-range magnetic ordering.[24] We have carried out ^{51}V NMR and NQR measurements below T_{MI}.[20]

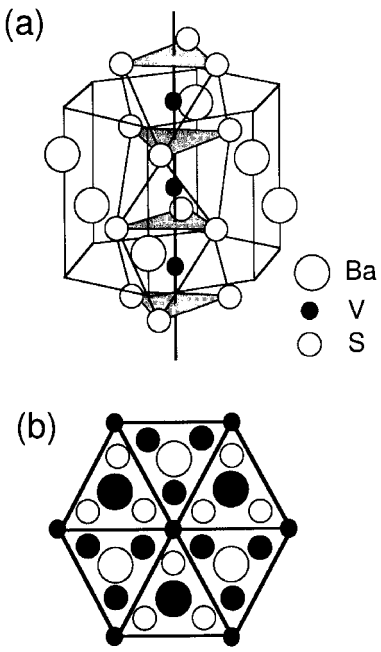

Fig. 15. The crystal structure of $BaVS_3$. V atoms form a one-dimensional (1D) chain along the c axis and form a triangular lattice in the basal plane as in (b). Open and hatched marks in (b) indicate above and below the V layer.

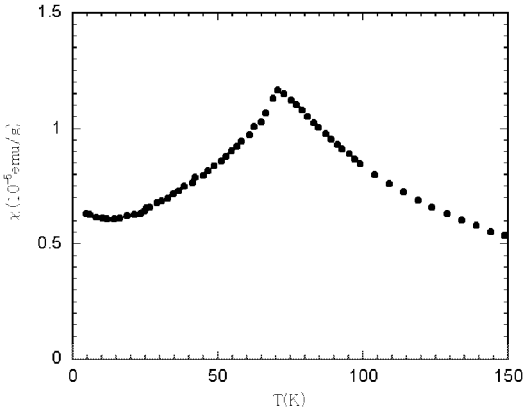

Fig. 16. The temperature dependence of the susceptibility for polycrystalline $BaVS_3$.

Figure 17 shows field-swept spectra at several temperatures, which were measured in the same conditions except temperature. Above 30 K, which will be denoted as T_X hereafter, we observed a sharp resonant peak, implying absence of a hyperfine field due to magnetic ordering. Around T_X, the peak intensity decreases rapidly and almost disappears at T_X. This decrease of the echo amplitude is ascribed to the divergent increase of spin-spin relaxation rate $1/T_2$ (note not $1/T_1$ at T_X. Below

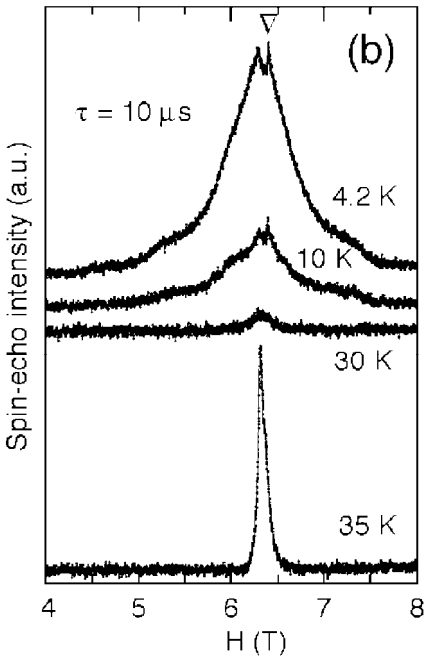

Fig. 17. Field-swept ^{51}V NMR spectra of $BaVS_3$ at several temperatures. The operating frequency is 70.5 MHz and pulse separation $\tau = 8$ μs. The profiles of broad peak below 30 K is explained by quadrupole effects with NQR parameters determined by NQR spectrum at 1.4 K (see Fig. 18). The sharp and small signal indicated by an open triangle is attributed to impurity phases.

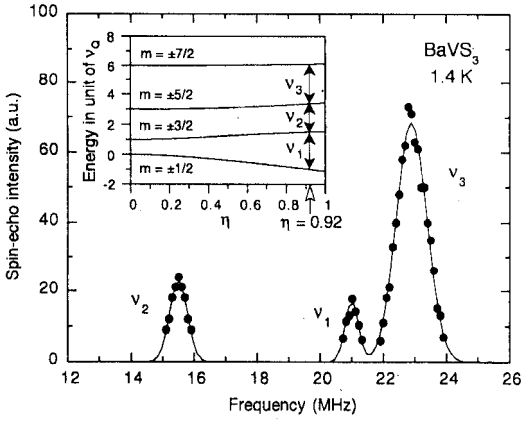

Fig. 18. The ^{51}V NQR spectrum for $BaVS_3$ measured at 1.4 K. The inset shows nuclear spin energies for $I = 7/2$ in nonaxial EFG as a function of η. The analysis gives $\nu_Q = 8.37 \pm 0.01$ MHz and $\eta = 0.916 \pm 0.001$.

T_X, we observed another type of signal which is much broader than that above T_X. A possible origin of the line broadening will be onset of hyperfine fields due to occurrence of some kind of magnetic ordering. However, we have shown that this broadening can be explained by a sudden increase of quadrupole effects.

Figure 18 shows the zero-field spin-echo spectrum at 1.4 K. We observed three peaks with different intensities. We have shown that the peak positions are well explained by ^{51}V NQR by assuming the pure quadrupole frequency $\nu_Q = 8.37$ MHz and the asymmetric parameter $\eta = 0.916$. Using these parameters, the broadening of the field-swept spectra below T_X is well explained by the quadrupole effect without introducing magnetic hyperfine field. From these observations, we have concluded that $BaVS_3$ does not have static spins at the ground state, and that extraordinary large and asymmetric electrical field gradient (EFG) at the V site, which is larger by one order than the possible magnitude for ionic V, exists at low temperatures.

It is very interesting that this large EFG suddenly disappears at $T_X \simeq 30$ K. The drastic variation in EFG can be ascribed only to intra-atomic ($3d$ electron) charge redistribution; from asymmetric below T_X to spherical above T_X. The appearance of the unspherical $3d$ cloud below T_X may be ascribed to the orbital ordering associated with the lifting of orbital degeneracy. The extraordinary large magnitude of EFG is probably related to the strong covalency between V and S. If we employ the model proposed by Pen et al.,[19] the anomaly is considered as the orbital ordering inherent to the $S = \frac{1}{2}$ triangular lattice; $3d$ electrons at different atomic sites occupy different orbitals and form dimer-like spin singlets within the ab plane. It should be noted that no anomaly has been observed at T_X in thermodynamic properties such as specific heat[25] and thermal expansion.[23] Nuclear magnetic relaxation measurements indicate a peculiar nature of the T_X-anomaly; the only spin-spin relaxation rate $1/T_2$ (not $1/T_1$) shows a divergence at T_X.[26] We interpret the T_X-anomaly as the dynamical effect, i.e., not a phase transition but a crossover, which is a result of fluctuations of orbitals. Above T_X, ^{51}V nucleus feels the average EFG, which is almost spherical, produced by asymmetric electron clouds. There remains, however, many unsolved problems in this system. What is the origin of metal-insulator transition? Does it associate with orbital ordering?

Very recently, we have found a new aspect of this material, that is, the appearance of magnetic Bragg peaks at

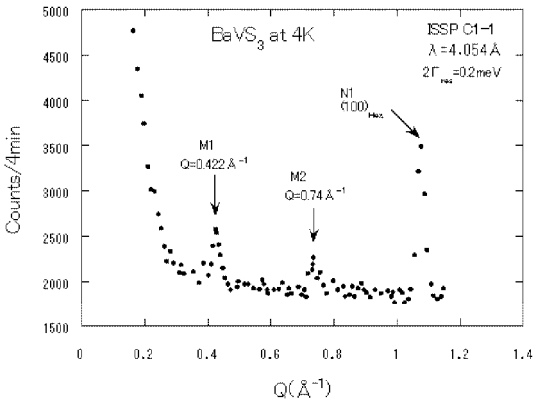

Fig. 19. Neutron diffraction pattern of $BaVS_3$ at 4K in low angle region. M1 and M2 peaks disappear above 30K, indicating magnetic origin.

low angles in powder neutron diffraction pattern below 30 K, implying the onset of long range antiferromagnetic order, which has been denied by a previous measurement.[24] The strongest peak locates at a very low angle corresponding to $Q = 0.422$ Å^{-1}, outside of the scanning angle of the previous measurements. The second, a little weaker, peak appears at $Q = 0.74$ Å^{-1}. (See Fig. 19) From these two peaks, we have concluded that there exist an incommensurate antiferromagnetic order with the magnetic propagation vector of (0.225 0.225 0) in the hexagonal Miller indices. Assuming spins rotate in c-plane, we roughly estimated the magnitude of V moment as $0.6\mu_{\mathrm{B}}$. It is interesting to note that long period incommensurate structures were found in ionic crystals with the same crystal structure such as $RbFeCl_3$[27] and $CsFeCl_3$ under applied fields.[28] For the latter case, it was reported that the magnetic propagation vector is $(\frac{1}{3} - \delta, \frac{1}{3} - \delta, 0)$, where $\delta = 0.01$.

Detection of magnetic peaks, however, gives rise to a serious inconsistency with NMR and NQR observations, which suggest absence of long-range magnetic order. There may be two interpretations to explain this dilemma. Firstly, a kind of charge ordering takes place in V ions and a part of V ions form singlet and others remain magnetic. The nonmagnetic V ions give NMR and NQR signals and magnetic ones form antiferromagnetic lattice. Such a charge ordering effect is often found in vanadium oxide compounds.[29] Another possibility is that the antiferromagnetic sublattice fluctuates faster than a NMR frequency ($\sim 10^{-7}$ sec) but slower than a neutron passing time ($\sim 10^{-12}$ sec). Discrepancy between NMR and neutron observations is found in $CsCoCl_3$ type frustrate compounds like $CsMnI_3$.[30] For this compound, neutron diffraction has revealed 120^{o} structure in the c plane canted along the c axis with Mn^{2+} full moment. On the other hand, ^{55}Mn nucleus feel only an axial component of the hyperfine field, which is much smaller than that expected for Mn^{2+} moment. In order to have a conclusion, we have to collect more experimental evidence. We have carried out inelastic neutron scattering above 30 K and found fairly strong inelastic magnetic scattering around $Q = 0.45$ Å^{-1} with $\Delta E \geq 1$ meV at 50 K. This means that the antiferromagnetic component with $Q \sim 0.45$ Å^{-1} fluctuates faster than the characteristic time of neutron diffraction. We believe that it is a challenging problem to reveal what T_{X} is.

Acknowledgements

The authors would like to thank many collaborators, Dr. H. Wada, Dr. H. Imai, Mr. R. Iehara of Kyoto University, Prof. K. Kakurai and Dr. M. Nishi of the University of Tokyo, Prof. M.Mekata of Fukui University.

1) A. P. Ramirez: Annu. Rev. Mater. Sci. 24 (1994) 453.
2) P. Fazekas and P. W. Anderson: Phil. Mag. 30 (1974) 423.
3) T. Moriya: J. Magn. Magn. Mater. 14 (1979) 1.
4) R. Ballou, J. Deportes, R. Lemaire, Y. Nakamura and B. Ouladdiaf: J. Magn. Magn. Mater. 70 (1987) 129.
5) M. Shiga, H. Nakamura and N. Metoki: J. Magn. Magn. Mater. 196-197 (1999) 751.
6) H. Nakamura, H. Wada, K. Yoshimura, M. Shiga Y. Nakamura, J. Sakurai and Y. Komura: J. Phys. F 18 (1988) 981.
7) H. Wada, M. Shiga, Y. Nakamura: Physica B 161 197.
8) R. A. Fisher R. Ballou, J. P. Emerson, E. Lelievre-Berna and N. E. Phillips: Proc. Int. Conf. Physics of Transition Metals, Darmstadt, p.830, World Scientific 1992.
9) E. Bauer, I. S. Dubenko, E. Gratz, R. Hauser, A. Markosyan and K. Payeral: Proc. Int. Conf. Physics of Transition Metals, Darmstadt, p.826, World Scientific 1992.
10) H. Imai. H. Wada and M. Shiga: J. Phys. Soc. Jpn. 64 (1995) 2198.
11) M. Shiga, H. Wada, Y. Nakamura, J. Deportes and K. R. A. Ziebeck: J. Physique 49 (1988) C8-241.
12) H. Nakamura, F. Takayanagi, M. Shiga, M. Nishi and K. Kakurai: J. Phys. Soc. Jpn. 65 (1996) 2779.
13) R. Ballou, E. Lelievre-Berna and B. Fak: Phys. Rev. Lett. 76 (1996) 2125.
14) B. Canals and C. Lacroix: Phys. Rev. Lett. 80 (1998) 2933.
15) C. Lacroix, C. Solontsov and R. Ballou: Phys. Rev. B 54 (1996) 15178.
16) M. Mekata, T. Asano, H. Nakamura, M. Shiga, K. Kojima, G. M. Luke, A. Keren, W. D. Wu, Y. J. Uemura, S. Dunsinger and M. Gingras: Hyperfine Interact. 104 (1997) 337.
17) Y. Takahashi: J.Phys.: Condens. Matter 2 (1990) 8405.
18) H. Nakamura, K. Yoshimoto, M. Shiga, M. Nishi and K. Kakurai: J. Phys.: Condens. Matter 9 (1997) 4701.
19) H. F. Pen, J. van den Brink, D. I. Khomskii and G. A. Sawatzky: Phys. Rev. Lett. 78 (1997) 1323.
20) H. Nakamura, H. Imai and M. Shiga: Phys. Rev. Lett. 79 (1997) 3779.
21) P. Fazekas: private communication
22) H. Nakamura, H. Tanahashi, H. Imai, M. Shiga, K. Kojima, K. Kakurai and M. Nishi: J. Phys. Chem. Solids 60 (1999) 1137.
23) F. Sayetat, M. Ghedira, J. Chenavas and M. Marezio: J. Phys. C 15 (1982) 1627.
24) M. Ghedira, M. Anne, J. Chenavas, M. Marezio and F.Sayetat: J.Phys. C 19 (1986) 6489.
25) H. Imai, H. Wada and M. Shiga: J. Phys. Soc. Jpn. 65 (1996) 3460.
26) H. Nakamura, H. Imai and M. Shiga: Physica B 259-264 (1999) 965.
27) N. Wada, K. Ubukoshi and K. Hirakawa: J. Phys. Soc. Jpn. 51 (1982) 2833.
28) W. Knop, M. Steiner and P. Day : J. Magn. Magn. Mater. 31-34 (1983) 1033.
29) T. Ohama, H. Yasuoka, M. Isobe and Y. Ueda: Phys. Rev. B 59 (1999) 3299.
30) T. Kubo, J. Miyakita and S. Maegawa : J. Magn. Magn. Mater. 177-181 (1998) 829.